RSC Advances

PAPER

View Article Online
View Journal | View Issue

Cite this: *RSC Adv.*, 2025, **15**, 42443

Label-free fluorescent probe based on upconversion nanoparticles for convenient detection of cytochrome c

Hong Zheng and Zhan Wu *

Received 28th June 2025
Accepted 13th October 2025

DOI: 10.1039/d5ra04602e

rsc.li/rsc-advances

Abnormal levels of cytochrome c (Cyt c) are closely associated with various human diseases, including neurodegenerative disorders and cancers. Therefore, the quantitative detection of Cyt c holds significant value for both disease diagnosis and therapeutic efficacy assessment. Herein, we developed two novel label-free fluorescent probes for sensitive Cyt c detection based on upconversion nanoparticles: one functionalized with poly (ethylene glycol) ylated phospholipid (DSPE-PEG) alone, and the other co-functionalized DSPE-PEG combined with triphenylphosphine. The electrostatic interaction generates resulting in a quantifiable fluorescence quenching effect. The proposed method demonstrated excellent performance in the detection of Cyt c in complex matrices, including cell lysates and human blood sample. Notably, it offers significant advantages over conventional assays by simplifying sample preparation, reducing operational steps, and providing rapid response with distinct observable signals, showing great potential for clinical diagnosis and therapeutic monitoring.

Introduction

Cytochrome c (Cyt c) is a water-soluble spherical protein and is closely related to apoptosis[1] and immune response.[2] It has distinct dynamic patterns in concentration and release, making it a promising biomarker for diagnosing various diseases. Previous studies have reported that serum levels of Cyt c are elevated in patients with inflammatory arthritis, liver disease, myocardial infarction and other diseases, while the expression level of Cyt c decreases in cancer tissues. Monitoring serum Cyt c levels can also provide valuable insights into postoperative disease evaluation.[3–6] For instance, breast cancer patients exhibiting high serum Cyt c expression tend to have a higher risk of recurrence.[7] Therefore, achieving highly sensitive and specific rapid detection of Cyt c holds significant importance in biological and medical research.

To date, numerous analytical techniques for Cyt c detection have been reported,[8] including flow cytometry,[9] western blotting,[10] enzyme-linked immunosorbent assay (ELISA),[11] chemiluminescence[12] and high-performance liquid chromatography (HPLC).[13] However, most of these methods have problems such as cumbersome detection steps, complex preparation processes, and being limited by large and expensive instruments. Electrochemical techniques have emerged as a powerful tool for detecting Cyt c, owing to their high sensitivity and capacity for quantitative analysis. For instance, Duan's group[14] developed a combined optical-electrochemical probe, while Zhang's team[15] reported a photoelectrochemical immunosensor based on Cu_3SnS_4 nanoflowers. Both approaches demonstrated excellent sensitivity and low detection limit. However, their practical application remains limited owing to the complex fabrication procedures and the relatively high costs. The use of functionalized nanoparticles is a common complementary technical solution. The Cu–Ce-aNEs nanozyme-based electrochemical sensor developed by Yang's team[16] has streamlined detection procedures to some extent while enhancing sensitivity. Nevertheless, this technique still faces some challenges such as complex synthesis procedures and poor long-term stability. In conclusion, it is critical to develop a highly sensitive, cost-efficient, and easy-to-fabricate sensor for rapid and reliable Cyt c detection.

Fluorescent probes are widely utilized as detection tools due to their high selectivity and minimal instrument dependency, making them indispensable in biomolecule detection, environmental monitoring, and food safety analysis.[17–19] For instance, Song's team[20] designed dual-functional carbon dots, while Packirisamy's team[21] developed RPE-AuNCs to detect Hg^{2+}. However, conventional probes such as metal nanoclusters and carbon dots are typically excited by UV or visible light and often suffer from high autofluorescence backgrounds, which can significantly interfere with detection signals.[22] Upconversion nanoparticles (UCNPs) are an ideal platform for biosensing applications due to their high signal-to-noise ratio, resistance to photobleaching, and minimal background interference and light scattering effects.[23–26] Leveraging these advantages, this study developed a label-free nanosensor based on poly (ethylene

Chemical Biology & Traditional Chinese Medicine Research (Ministry of Education of China), Key Laboratory of Phytochemical R&D of Hunan Province, College of Chemistry and Chemical Engineering, Hunan Normal University, Changsha 410081, P. R. China. E-mail: zhanwu@hunnu.edu.cn

glycol) ylated phospholipid (DSPE-PEG) and triphenylphosphine (TPP) modified UCNPs for Cyt c detection. The detection mechanism of the sensor relies on the negative charge of the nanoprobe endowed by the DSPE-PEG modification, allowing it to bind to positively charged Cyt c (isoelectric point [pI] 10.0) by electrostatic interactions. The ingeniously designed molecular conformation of Cyt c enables it to function as a natural quencher,[27,28] facilitating rapid electron transfer and subsequent fluorescence quenching. Based on this fluorescence signal change, the visual quantitative detection of Cyt c was achieved. We employed lipophilic cation TPP[29] for charge balance, preventing excessive negative charge from DSPE-PEG modification that could impair Cyt c detection sensitivity. This dual-modification strategy provides complementary benefits. DSPE-PEG enhances nanoparticle stability and biocompatibility while effectively minimizing non-specific adsorption,[30] whereas TPP improves sensitivity in complex biological samples. It is worth noting that electrostatic adsorption-based detection strategies are not uncommon. For example, Yang's mitochondrial adenosine triphosphate (ATP) detection[31] and Zhang's lysozyme sensing system.[32] Based on previous reports,[33,34] electrostatic interaction is a common mechanism for sensing. This tool combines practical advantages including simple preparation, operational convenience, good cost-efficiency, rapid response (<10 min), stable performance and excellent selectivity, making it particularly suitable for Cyt c monitoring in the medical field.

Experimental

Materials and reagents

$Gd(CF_3COO)_3$, $Yb(CF_3COO)_3$, $Tm(CF_3COO)_3$, CF_3COONa, oleic acid (OA, 90%), 1-octadecene (OED, 95%), oleylamine (OM, 90%), Cyt c and ATP were purchased from Sigma-Aldrich of Merck Group in Germany. Ethanol and myoglobin were purchased from Tansoole (Shanghai, China). Cyclohexane and chloroform were provided by Shanghai Sinopharm Group. All chemicals were purchased from Aladdin (Shanghai, China), including bovine serum albumin (BSA), insulin (INS), ascorbic acid (AA), hemoglobin, L-arginine and various salts (potassium chloride, magnesium chloride, disodium hydrogen phosphate, sodium dihydrogen phosphate, sodium chloride, potassium bromide). Additionally, horseradish peroxidase (HRP) was purchased from Shanghai yuanye Bio-Technology Co., Ltd. DSPE-mPEG2000 was purchased from Xi'an Ruixi Biotechnology, DSPE-PEG2000-TPP from Xi'an Qiyue Biology, RIAP lysate, lysozyme from Beyotime (Shanghai, China), and protease inhibitor Cocktail from Bimake (Shanghai, China). A549 cells and HeLa cells were purchased from the ATCC cell Bank (United States). All chemicals employed in this study were analytical-grade reagents and were utilized without additional purification.

Preparation of UCNPs

The UCNPs were synthesized *via* the high-temperature thermal decomposition method.[35] At room temperature, $Gd(CF_3COO)_3$ (0.29 mmol), $Yb(CF_3COO)_3$ (0.70 mmol), $Tm(CF_3COO)_3$ (0.01 mmol), CF_3COONa (1 mmol), OA (20 mmol), OM (20 mmol), and ODE (40 mmol) were introduced into a three-neck flask (100 mL). It was heated in a stepwise manner to 120 °C with stirring until oxygen and low-boiling components were removed under vacuum. Under the protection of N_2, the temperature was raised to 320 °C for 1 hour. After cooling to room temperature, the products were precipitated with ethanol. The resulting precipitate was collected through centrifugation (8000 rpm, 8 min) and subsequently re-dispersed in 10 mL of cyclohexane to obtain the α-phase $NaGdF_4$:Yb/Tm. Then, $Gd(CF_3COO)_3$ (0.145 mmol), $Yb(CF_3COO)_3$ (0.35 mmol), $Tm(CF_3COO)_3$ (0.005 mmol), CF_3COONa (0.5 mmol), OA (20 mmol), ODE (20 mmol) were mixed with 5 mL of α-phase $NaGdF_4$:Yb/Tm to synthesize the β-phase $NaGdF_4$:Yb/Tm. Then, $Gd(CF_3COO)_3$ (1 mmol), CF_3COONa (1 mmol), OA (20 mmol), ODE (20 mmol) were combined with 5 mL of β-phase $NaGdF_4$:Yb/Tm to prepare the $NaGdF_4$:Yb/Tm@$NaGdF_4$. The synthesis steps were the same as above.

Construction of upconversion nanofluorescent probes

The Lipo-UCNPs were synthesized according to the reported method.[36] A 200 μL of 20 mg mL^{-1} UCNPs and cyclohexane (1 mL) were added to a round-bottom flask (10 mL). Under reduced pressure conditions, cyclohexane was completely removed by using a rotary evaporator. The mass of UCNPs was determined by the differential weighing method. Subsequently, DSPE-PEG with an equal mass of UCNPs was added and dissolved in 2 mL of chloroform. After performing rotary evaporation at room temperature under reduced pressure, a thin lipid film was formed on the inner wall of the flask. The addition of ultrapure water (2 mL) followed by vigorous sonication at 70 °C yielded water-soluble Lipo-UCNPs. In accordance with reference,[37] a series of varying masses of DSPE-PEG-TPP was combined with Lipo-UCNPs, maintaining mass ratios of 1 : 2, 1 : 1, and 2 : 1 for DSPE-PEG-TPP to Lipo-UCNPs. The mixture was then rotated overnight at 4 °C to facilitate the modification of TPP on the surface of Lipo-UCNPs. Purification of Lipo-TPP-UCNPs was accomplished through ultracentrifugation (15 000 rpm, 6 min) and washing. The purified nanoparticles were then resuspended in 2 mL of ultrapure water and stored at 4 °C for subsequent use.

In vitro measurement of Cyt c

To assess the feasibility of Lipo-UCNPs, we took 10 μLof phosphate buffered saline (PBS, 135 mM NaCl, 4.7 mM KCl, 10 mM Na_2HPO_4, 2 mM NaH_2PO_4, pH 7.4), 40 μL of Lipo-UCNPs and 50 μL of Cyt c (200 μM) in polyethylene tubes. The mixture was incubated in a 37 °C water bath for 1.5 hours. Fluorescence measurements were performed using a fluorescence spectrometer (HORIBA FluoroMax-4, Japan) equipped with a 980 nm near-infrared excitation source (power 2 W). We established a series of Cyt c concentration gradients. Fluorescence signals were collected following the same experimental procedure, and a concentration-fluorescence intensity standard curve was established. For selectivity analysis, Cyt c was substituted with

potential interfering substances within the same reaction system. Potential interferents were systematically evaluated under the following concentrations: AA, glucose, L-arginine, and lysozyme (200 μM); KCl and $MgCl_2$ (100 mM); ATP (10 mM); BSA, hemoglobin, myoglobin, and HRP (1 mg mL^{-1}); and INS (3 mg mL^{-1}). Then we incubated the nanoparticles in PBS buffer (pH 7.4) and RPMI 1640 medium, both supplemented with 10% fetal bovine serum (FBS). We monitored changes in particle hydrodynamic diameter and polydispersity index (PDI) over time. We prepared buffer solutions at varying pH levels: citrate buffer (pH 4, 5, 6), PBS (pH 7, 7.4, 8), and tris–HCl (pH 9), along with sodium chloride solutions (100 – 500 mM in 100 mM increments). Subsequently, 100 μL of each buffer (or sodium chloride solution) was incubated with 50 μL of Lipo-UCNPs (1 mg mL^{-1}) at 37 °C for 1.5 hours. Fluorescence intensity was measured to assess the effects of pH and ionic strength on electrostatic adsorption.

Preparation of cell lysates and blood sample

To evaluate the universality of probe detection, we utilized A549 cells for Lipo-UCNPs and HeLa cells for Lipo-TPP-UCNPs. A549 cells (1×10^5 cells per well) were cultured in 6-well plates and incubated in RPMI 1640 medium at 37 °C with 5% CO_2 for 24 hours. Then, the old medium was removed, followed by three washes with ice-cold DPBS. The RPIA lysate (100 μL) and cocktail protease inhibitor (1 μL) mixture were added, shaken on a shaker (15 min). Proteins were transferred into a centrifuge tube using a cell scraper, followed by centrifugation (4 °C, 12 000 rpm, 10 min) to collect the supernatant as the protein mixture. HeLa cells were treated as above. Human blood sample was obtained from a healthy volunteer using a vacuum blood collection tube. The sample was centrifuged at 3000 rpm for 10 min at 4 °C to separate the serum. The supernatant (serum) was carefully collected, aliquoted, and stored at −80 °C until use. For the detection of Cyt c, the frozen serum was thawed on ice and diluted 2-fold with PBS (pH 7.4) to reduce background interference from the complex matrix.

Results and discussion

Characterization of UCNPs

The synthesized UCNPs were characterized. As shown in the transmission electron microscopy (TEM) image of Fig. 1A, the UCNPs exhibit excellent dispersibility and uniformity. High-resolution transmission electron microscopy (HR-TEM) (Fig. 1B) revealed continuous lattice fringes with consistent crystallographic orientation, which strongly indicates the preservation of structural integrity. The elemental composition was further validated by energy dispersive spectroscopy (EDS) analysis (Fig. 1C) and element mappings (Fig. 1D), confirming the presence of Na, Tm, Yb, Gd, and F. These results also highlight the predominant content of Gd (highest) and the minimal incorporation of Tm (lowest). This finding is consistent with the initial feed ratios utilized during material synthesis process. Compared to the X-ray powder diffractometer (XRD) pattern of pure hexagonal-phase $NaYF_4$ (Fig. S1), the

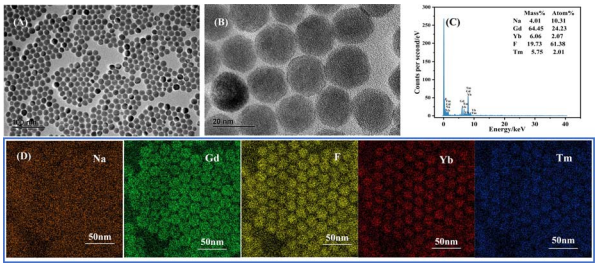

Fig. 1 Morphological, structural, and elemental characterization of UCNPs. (A) The TEM image of UCNPs ($NaGdF_4$:Yb/Tm@$NaGdF_4$). Scale bar, 100 nm; (B) HR-TEM image revealing the crystal structure of UCNPs. Scale bar, 20 nm; (C) energy spectrum and corresponding elemental composition analysis of UCNPs; (D) the element mapping images of UCNPs, showing the distribution of Na, Tm, Yb, Gd, and F elements. Scale bar, 50 nm.

UCNPs exhibit a shift to smaller angles due to the substitution of Y by Gd. This substitution increases the atomic radius, expands the lattice volume, and widens the lattice spacing, thereby causing the overall diffraction peaks to shift leftward. These results collectively verify the successful synthesis of $NaGdF_4$:Yb/Tm@$NaGdF_4$.

Characterization of upconversion nanofluorescent probes

Dynamic light scattering (DLS) analysis revealed significant changes in nanoparticle following DSPE-PEG modification (Fig. 2A). The hydrodynamic diameter increased from approximately 85 nm (PDI 0.126) to 100 nm (PDI 0.172). It is demonstrated that Lipo-UCNPs still possess good dispersibility and there is no obvious aggregation. As shown in the zeta potential measurements (Fig. 2B), the potential of the modified nanoprobe shifts from +22.23 mV to −12.633 mV. It indicates that Cyt c can easily bind to the nanoprobe. According to the analysis of emission spectra (Fig. 2C), it is evident that both exhibit

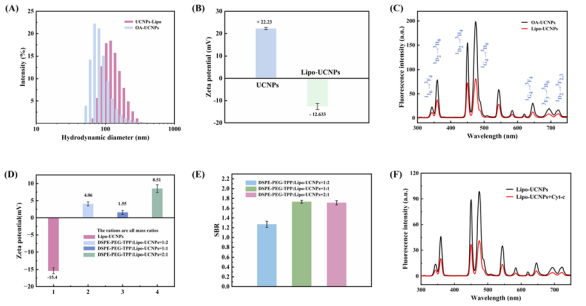

Fig. 2 Characterizations of nanoparticle surface modification and functionalization. (A) DLS analysis of nanoparticles before and after DSPE-PEG modification; (B) the zeta potential of nanoparticles pre- and post-DSPE-PEG modification. All plots show mean ± SD for $n = 3$ replicates; (C) the fluorescence spectra of UCNPs (black line) and Lipo-UCNPs (red line); (D) the zeta potentials of Lipo-UCNPs modified with different mass ratios of DSPE-PEG-TPP. All plots show mean ± SD for $n = 3$ replicates; (E) signal-to-background ratio of Lipo-UCNPs with varying DSPE-PEG-TPP modification levels; (F) the fluorescence spectra of Lipo-UCNPs before and after addition of Cyt c (200 μM) to evaluate feasibility.

prominent characteristic peaks at 344 nm, 360 nm, 450 nm, 474 nm, 645 nm, 695 nm and 723 nm. This is attributed to $^1I_6 \rightarrow {}^3F_4$, $^1D_2 \rightarrow {}^3H_6$, $^1D_2 \rightarrow {}^3F_4$, $^1G_4 \rightarrow {}^3H_6$, $^1G_4 \rightarrow {}^3F_4$, $^3F_3 \rightarrow {}^3H_6$ and $^1D_2 \rightarrow {}^3F_{2,3}$ transitions. This result demonstrates that DSPE-PEG functionalization effectively enhances biocompatibility while maintaining the probe's fluorescence emission position. The increased hydrodynamic diameter, altered potential, and slight fluorescence attenuation collectively confirmed the successful DSPE-PEG conjugation.

We optimized the amount of TPP in Lipo-TPP-UCNPs to achieve optimal performance. As a lipophilic cation, TPP confers a positive charge to the nanoparticles. As illustrated in Fig. 2D, the potential of nanoprobes with varying ratios shifts from negative to positive. Additionally, probes with a higher modification concentration exhibit distinct peak absorption at 220–240 nm in the UV-Vis spectra (Fig. S2). These findings collectively indicate that TPP has been successfully modified onto the surface of the UCNPs. In the detection of Cyt c, all three different modification ratios demonstrated good feasibility. Taking all factors into consideration, we selected 1 : 1 modified probes with high signal-to-noise ratios (Fig. 2E) for the subsequent experiments.

Feasibility analysis of upconversion nanofluorescent probes

The interaction between upconversion nanofluorescent probes and Cyt c was characterized by notable fluorescence quenching, as shown in Fig. 2F. It provides an initial confirmation of the probe's detection capability. Additionally, we investigated the effect of incubation time on fluorescence intensity. As shown in Fig. S3, fluorescence quenching occurs within a relatively short time (less than 10 min). The quenching efficiency progressively increased with the reaction time. After approximately 90 min of incubation, the fluorescence quenching reaches the maximum. Therefore, we selected 90 min as the optimal reaction time for subsequent experiments. Ensuring complete probe-analyte interaction while preserving experimental efficiency.

Stability and specificity of upconversion nanofluorescent probes

We further examined the stability of the upconversion nanofluorescent probes. As shown in Fig. 3A, the hydrodynamic diameter of the nanoparticles remained stable in PBS, varying from 98.5 to 108.6 nm (average error is 3.384) in 48 hours. Similarly, in complete cell culture medium, the diameters stayed between 99.6 and 104.3 nm (average error is 3.872). As shown in Fig. 3B, the PDI was low in PBS, it ranged from 0.216 to 0.254 (average error is 0.016), and in cell culture medium, from 0.192 to 0.298 (average error is 0.030). At pH values ranging from 4 to 9 (Fig. 3C) and concentrations ranging from 100 to 500 mM (Fig. 3D), the fluorescence intensity of the nanoparticles remained relatively stable. These results indicate that our sensing system possesses excellent anti-interference capability against ionic strength and is suitable for applications in physiological samples. Furthermore, we observed that the fluorescence intensity of the samples remained stable (Fig. S4) for at least one month when stored under dark conditions at

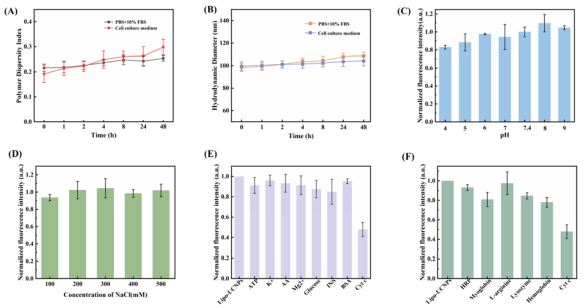

Fig. 3 Characterization and application performance of upconversion nanofluorescent probes in physiological conditions. (A) The hydrodynamic diameter and (B) PDI of nanoparticles in PBS and cell culture medium (both containing 10% FBS);(C) the fluorescence intensity of Lipo-UCNPs at 473 nm under conditions of pH 4, 5, 6, 7, 7.4, 8 and 9; (D) the fluorescence intensity of Lipo-UCNPs at 473 nm in solutions of different concentrations of NaCl (100–500 mM); (E) fluorescence response of Lipo-UCNPs to ATP (10 mM), K^+ (100 mM), AA (200 μM), Mg^{2+} (100 mM), glucose (200 μM), INS (3 mg mL^{-1}), BSA (1 mg mL^{-1}) and Cyt c (200 μM) at 475 nm; (F) fluorescence response of Lipo-UCNPs to HRP (1 mg mL^{-1}), myoglobin (1 mg mL^{-1}), L-arginine (200 μM), lysozyme (200 μM), Cyt c (200 μM) and hemoglobin (1 mg mL^{-1}) at 475 nm. Error bars represent the standard deviations from three sets of repeated measurements.

4 °C in sealed containers and avoided repeated freezing and thawing. These findings suggest a promising potential for commercialization to some extent. The physical and functional stability of the probe confirms its considerable commercial potential.

To verify the detection specificity for Cyt c, we investigated potential interference from various biological components that may coexist with Cyt c in physiological environments. The nanoprobes were co-incubated with various potential interferents, including BSA, ascorbic acid, ATP, insulin, glucose, potassium ions, and magnesium ions. After normalization to the intrinsic fluorescence of the nanoprobes, no significant quenching was observed (Fig. 3E). This result demonstrates that the nanoprobes exhibit specificity for detecting Cyt c. To further validate selectivity, we selected hemoglobin, myoglobin, and HRP which like Cyt c also contain iron porphyrin. In addition, two high isoelectric point proteins, L-arginine (pI 10.76) and lysozyme (pI 11.0), were also included in the evaluation. As we expected none of these biomolecules induced significant fluorescence quenching (Fig. 3F). These results show that neither structurally similar porphyrin analogs nor cationic biomolecules induce fluorescence quenching, confirming the high selectivity and reliability of our detection system.

Detection performance of upconversion nanofluorescent probes

To evaluate the sensitivity and detection limit of this strategy, we conducted an analysis of fluorescence signals at varying concentrations of Cyt c. As illustrated in Fig. 4A, the fluorescence intensity exhibited a concentration-dependent decrease. This reduction in fluorescence signal is attributed to the quenching effect of Cyt c. Within the 20 μM to 100 μM range,

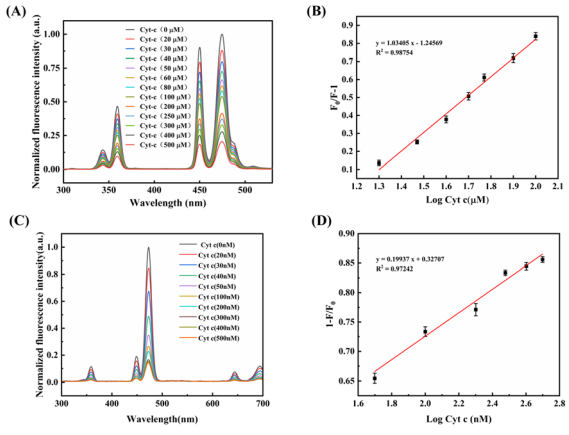

Fig. 4 Concentration-dependent fluorescence response and calibration curves of upconversion nanofluorescent probes to Cyt c. (A) The fluorescence spectra of Lipo-UCNPs as a function of Cyt c concentration (0–500 μM); (B) standard curve of Lipo-UCNPs fluorescence intensity at 475 nm as a function of Cyt c concentration (R^2 = 0.98754), error bars represent standard deviations; (C) the fluorescence spectra of Lipo-UCNPs as a function of Cyt c concentration (0–500 nM); (D) standard curve of Lipo-TPP-UCNPs fluorescence intensity at 473 nm as a function of Cyt c concentration (R^2 = 0.97242). Data are presented as mean ± SD of n = 3 independent replicates.

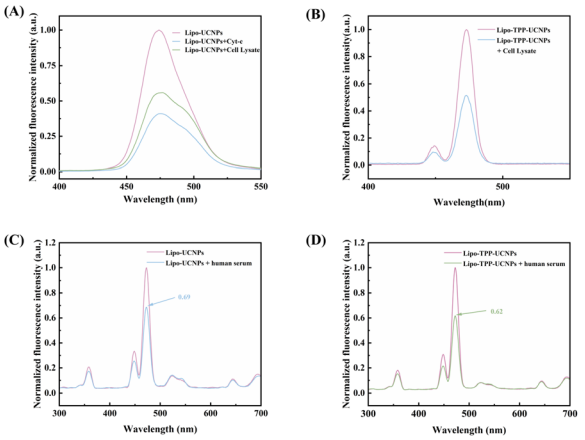

Fig. 5 Fluorescence response of upconversion nanofluorescent probes in complex biological samples. (A) Fluorescence emission spectra of Lipo-UCNPs, Lipo-UCNPs with Cyt c, Lipo-UCNPs with cell lysate under control conditions; (B) fluorescence emission spectra of Lipo-TPP-UCNPs, Lipo-TPP-UCNPs with cell lysate; (C) the fluorescence detection of Lipo-UCNPs and (D) Lipo-TPP-UCNPs in blood samples. All spectra were recorded in PBS at room temperature.

there exists a strong linear correlation between the fluorescence quenching effect at 475 nm and the concentration of Cyt c (Fig. 4B). The linear regression equation is $y = 1.03405\ x = 1.24569$. The limit of detection (LOD) was determined to be 19.40 μM, calculated as three times the standard deviation of the blank sample's fluorescence signal divided by the slope of the linear regression. As depicted in Fig. 4C, Lipo-TPP-UCNPs also demonstrated a robust response and effective discrimination across different concentrations of Cyt c. Within the concentration range of 20–50 nM (Fig. S5) and 50–500 nM (Fig. 4D), a strong linear relationship was observed between fluorescence intensity and Cyt c concentration. This association makes the method suited for postoperative detection of diseases with severely reduced Cyt c expression, such as cancer.[38] Collectively, the results indicate that the nanoprobes have excellent analytical performance for Cyt c.

Analytical applications of upconversion nanofluorescent probes in cell lysates and blood sample

Low cytotoxicity is a critical prerequisite for the application of probes in fields such as medical diagnostics. By MTS assay (3 – (4,5-dimethylthiazol – 2-yl) – 5 – (3 – carboxymethoxyphenyl) – 2-(4-sulfophenyl) – 2H – tetrazolium), we observed that cell viability remained unaffected even when the probe concentration reached 150 μg mL^{-1} for 8 hours (Fig. S6). This suggests that the synthesized probe has low cytotoxicity, thereby minimizing potential risks to operators during detection.

To validate the practical application of the probes, we conducted an experiment utilizing upconversion nanofluorescent probes to detect Cyt c in complex biological matrices. Incubation of Lipo-UCNPs with lysates from 1 × 10^5 A549 cells produced significant fluorescence quenching (Fig. 5A), consistent with results obtained from control experiments using purified Cyt c. Similarly, the incubation of 1 × 10^5 HeLa cell lysates with Lipo-TPP-UCNPs also resulted in pronounced fluorescence quenching (Fig. 5B). These indicate that the probe can be used for detection in different cellular environments. To further validate the detection performance of the probe, we conducted an additional evaluation of its performance in human blood sample. Upon simultaneous incubation of both Lipo-UCNPs and Lipo-TPP-UCNPs with the same blood sample, and subsequent normalization of their fluorescence intensities for comparison between Fig. 5C and D. It showed Lipo-TPP-UCNPs have a stronger fluorescence quenching signal than Lipo-UCNPs. This is likely attributed to the fact that under normal physiological conditions, Cyt c is primarily localized in the mitochondrial intermembrane space. The mitochondrial targeting capability of TPP, which promotes probe interaction with mitochondrial-localized Cyt c. Taken together, these results collectively demonstrate that the probe is capable of effectively performing detection in real complex samples.

Exploration of the sensing mechanism

To clarify the sensing mechanism between the probes and Cyt c, we referred to the research conducted by the Fan group[39] on the efficient quenching mechanism of Cyt c and conjugated polymers. Inspired by this work, we applied Stern–Volmer analysis (Fig. S7) to the fluorescence response of Lipo-UCNPs to varying Cyt c concentrations. The fitting result, $F_0/F = 0.00917 + 0.98743$ [Cyt c], yielded a quenching constant K_s of 9170 M^{-1}. Fluorescence lifetime measurements (Fig. 6A) revealed that the lifetime remained virtually unchanged with increasing Cyt c concentration, which is a characteristic of static quenching. In addition, the absence of spectral overlap between the UV absorption of Cyt c and the fluorescence emission of UCNPs (Fig. 6B) ruled out the possibility of fluorescence resonance energy transfer.

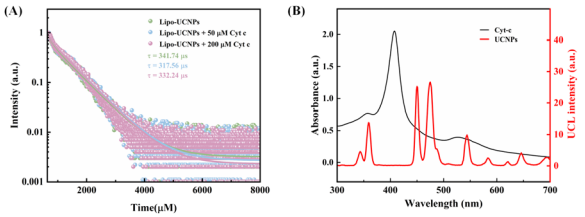

Fig. 6 Spectroscopic characterization for sensing mechanism investigation. (A) The fluorescence lifetime of the up-conversion nanofluorescent probe changes with the different concentrations of Cyt c (0 nM, 50 nM, 200 nM); (B) absorption spectrum of Cyt c and fluorescence spectrum of UCNPs.

Based on the experimental results and considering the electrostatic interaction between the negatively charged Lipo-UCNPs and the positively charged Cyt c, we infer that the fluorescence quenching mechanism of the probe likely conforms to ultrafast photoinduced electron transfer (ET) coupled with static quenching driven by electrostatic attraction.

Conclusions

In summary, we have successfully constructed the label-free upconversion nanoprobes for the sensitive and selective detection of Cyt c. Importantly, beyond the demonstration of detection in standard buffers, we validated the practical applicability of this probe in biologically relevant environments (cell lysates and human blood), a crucial step toward real-world clinical translation. The simplicity and cost-effectiveness of this platform position it as a promising tool for point-of-care testing (POCT). Looking forward, future work will focus on further simplifying the detection workflow into a portable device and expanding the panel of detectable biomarkers based on this versatile nanoplatform for multiplexed disease diagnosis and management.

Ethical statement

All experiments were performed in accordance with the Guidelines of Hunan Normal University, and experiments were approved by the ethics committee at Hunan Normal University (Approval No.: 2025807). Informed consents were obtained from human participants of this study.

Author contributions

Hong Zheng: writing – original draft, methodology, data curation, formal analysis, writing – review & editing. Zhan Wu: writing – review & editing, supervision, conceptualization.

Conflicts of interest

The authors declare that they have no known competing financial interests or personal relationships that could have appeared to influence the work reported in this paper.

Data availability

The data supporting this article have been included as part of the manuscript. For requests about the original data, please do not hesitate to contact the corresponding author.

Supplementary information: crystal structure analysis (XRD) of the core–shell $NaGdF_4$:Yb/Tm@$NaGdF_4$ upconversion nanoparticles; UV-vis characterization of the TPP-modified probes; optimization data for the incubation time and stability assessment of the probes; linear detection range and Stern–Volmer analysis for cytochrome c quantification; cytotoxicity evaluation of the probes using A549 cells. See DOI: **https://doi.org/10.1039/d5ra04602e**.

Acknowledgements

The authors thank the National Science Foundation of China (91953105, 22274049) and Hunan province college students research learning and innovative experiment project (S202410542186) for supporting the study.

References

1 J. M. Song, P. M. Kasili, G. D. Griffin and T. Vo-Dinh, *Anal. Chem.*, 2004, **76**, 2591–2594.
2 A. Gouveia, E. Bajwa and A. Klegeris, *Biochim. Biophys. Acta Gen. Subj.*, 2017, **1861**, 2274–2281.
3 B. Alshehri, *Saudi Pharm. J.*, 2024, **32**, 102194.
4 Z. Zhou, T. Arroum, X. Luo, R. Kang, Y. J. Lee, D. Tang, M. Hüttemann and X. Song, *Cell Death Differ.*, 2024, **31**, 387–404.
5 Q. Wen, X. Zhang, J. Cai and P. H. Yang, *Analyst*, 2014, **139**, 2499–2506.
6 M. S. Chimenti, F. Sunzini, L. Fiorucci, E. Botti, G. L. Fonti, P. Conigliaro, P. Triggianese, L. Costa, F. Caso, A. Giunta, M. Esposito, L. Bianchi, R. Santucci and R. Perricone, *Front. Immunol.*, 2018, **9**, 2363.
7 S. Zhao, W. Shen, R. Du, X. Luo, J. Yu, W. Zhou, X. Dong, R. Gao, C. Wang, H. Yang and S. Wang, *Cancer Med.*, 2019, **8**, 593–605.
8 P. Manickam, A. Kaushik, C. Karunakaran and S. Bhansali, *Biosens. Bioelectron.*, 2017, **87**, 654–668.
9 C. B. Campos, B. A. Paim, R. G. Cosso, R. F. Castilho, H. Rottenberg and A. E. Vercesi, *Cytometry A*, 2006, **69**, 515–523.
10 J. J. Bass, D. J. Wilkinson, D. Rankin, B. E. Phillips, N. J. Szewczyk, K. Smith and P. J. Atherton, *Scand. J. Med. Sci. Sports*, 2017, **27**, 4–25.
11 J. Radhakrishnan, R. Origenes, G. Littlejohn, S. Nikolich, E. Choi, S. Smite, L. Lamoureux, A. Baetiong, M. Shah and R. J. Gazmuri, *Biomark. Insights*, 2017, **12**, 1177271917746972.
12 C. Liu, L. Ren, X. Li, N. Fan, J. Chen, D. Zhang, W. Yang, S. Ding, W. Xu and X. Min, *Biosens. Bioelectron.*, 2022, **207**, 114207.
13 S. I. Dikalov and D. G. Harrison, *Antioxid. Redox Signaling*, 2014, **20**, 372–382.

14 Z. Duan, Y. Ouyang, Y. Fu, F. Huang, F. Xia and I. Willner, *Angew. Chem., Int. Ed.*, 2023, **62**, e202301476.
15 X. Zhang, L.-H. Jin, Y.-Y. Li, Z.-Z. Xiao, Y. Feng, Y.-W. Lin and Y. Zhang, *Inorg. Chem. Front.*, 2023, **10**, 5591–5601.
16 H. Yang, J. Du, W. Wang, T. Li, R. Zhang, Y. Yu, K. Li and Y. Lin, *Talanta*, 2025, **282**, 126945.
17 P. Sun, M. Shang, R. Xie, Y. Gao, M. Tian, Q. Dai, F. Zhang and F. Chai, *Food Chem.*, 2024, **445**, 138794.
18 Y. Hao, F. Ji, T. Li, M. Tian, X. Han and F. Chai, *Food Chem.*, 2024, **446**, 138843.
19 L. Liu and A. Corma, *Trends Chem.*, 2020, **2**, 383–400.
20 Y. Song, R. Xie, M. Tian, B. Mao and F. Chai, *J. Hazard. Mater.*, 2023, **457**, 131683.
21 V. Packirisamy, B. Ayyadurai, D. Perumal, P. Pandurangan, J. K. Ranishree, P. Dhandapani and T. Nallamuthu, *J. Mater. Res.*, 2023, **38**, 3009–3021.
22 J. S. Anjali Devi, S. Madanan Anju, G. M. Lekha, R. S. Aparna and S. George, *Nanoscale Horiz.*, 2024, **9**, 1683–1702.
23 A. Gnach and A. Bednarkiewicz, *Nano Today*, 2012, **7**, 532–563.
24 D. Xu, C. Li, W. Li, B. Lin and R. Lv, *Front Chem.*, 2023, **11**, 1036715.
25 K. Binnemans, *Chem. Rev.*, 2009, **109**, 4283–4374.
26 H. Dong, S.-R. Du, X.-Y. Zheng, G.-M. Lyu, L.-D. Sun, L.-D. Li, P.-Z. Zhang, C. Zhang and C.-H. Yan, *Chemical Rev.*, 2015, **115**, 10725–10815.
27 D. Liao, J. Chen, W. Li, Q. Zhang, F. Wang, Y. Li and C. Yu, *Chem. Commun.*, 2013, **49**, 9458–9460.
28 Y. Ma, H. Bai, C. Yang and X. Yang, *Analyst*, 2005, **130**, 283–285.
29 J. Zielonka, J. Joseph, A. Sikora, M. Hardy, O. Ouari, J. Vasquez-Vivar, G. Cheng, M. Lopez and B. Kalyanaraman, *Chem. Rev.*, 2017, **117**, 10043–10120.
30 J.-C. Boyer, M.-P. Manseau, J. I. Murray and F. C. J. M. van Veggel, *Langmuir*, 2010, **26**, 1157–1164.
31 B. Yang, R. Tian, T. Guo, W. Qu, J. Lu, Y. Li, Z. Wu, S. Yan, Z. Geng and Z. Wang, *Anal. Chem.*, 2023, **95**, 5034–5044.
32 H. Zhang, P. Liu, H. Wang, X. Ji, M. Zhao and Z. Song, *Anal. Bioanal. Chem.*, 2021, **413**, 1541–1547.
33 H. Li, M. Yang, D. Kong, R. Jin, X. Zhao, F. Liu, X. Yan, Y. Lin and G. Lu, *Sensor. Actuator. B Chem.*, 2019, **282**, 366–372.
34 H. Bayraktar, C.-C. You, V. M. Rotello and M. J. Knapp, *J. Am. Chem. Soc.*, 2007, **129**, 2732–2733.
35 J. Zhao, J. Gao, W. Xue, Z. Di, H. Xing, Y. Lu and L. Li, *J. Am. Chem. Soc.*, 2018, **140**, 578–581.
36 Y. Cen, Y. M. Wu, X. J. Kong, S. Wu, R. Q. Yu and X. Chu, *Anal. Chem.*, 2014, **86**, 7119–7127.
37 C. Ren, D. Li, Q. Zhou and X. Hu, *Biomaterials*, 2020, **232**, 119752.
38 J. Javid, R. Mir, P. K. Julka, P. C. Ray and A. Saxena, *Tumor Biol.*, 2015, **36**, 4253–4260.
39 C. Fan, K. W. Plaxco and A. J. Heeger, *J. Am. Chem. Soc.*, 2002, **124**, 5642–5643.